Inorg. Chem. **2005**, *44*, 8979–8987

Gadolinium and Neodymium Citrates: Evidence for Weak Ferromagnetic Exchange between Gadolinium(III) Cations

Ricardo Baggio,[†] Rafael Calvo,*[,‡] María Teresa Garland,[#] Octavio Peña,[&] Mireille Perec,*[,§] and Alberto Rizzi[‡]

Departamento de Física, Comisión Nacional de Energía Atómica, Av. Gral. Paz 1499, 1650 San Martín, Buenos Aires, Argentina, Departamento de Física, Facultad de Bioquímica y Ciencias Biológicas, Universidad Nacional del Litoral and INTEC (CONICET-UNL), Güemes 3450, 3000 Santa Fe, Argentina, Departamento de Física, Facultad de Ciencias Físicas y Matemáticas, Universidad de Chile, Av. Blanco Encalada 2008, Casilla 483, Santiago, Chile, L.C.S.I.M. UMR 6511 CNRS, Institut de Chimie de Rennes, Université de Rennes 1, 35042 Rennes, Cedex, France, and Departamento de Química Inorgánica Analítica y Química Física, Facultad de Ciencias Exactas y Naturales, INQUIMAE, Universidad de Buenos Aires, Ciudad Universitaria, Pabellón II, 1428, Buenos Aires, Argentina

Received June 20, 2005

A new lanthanide citrate motif of general formula $[Ln(Hcit)(H_2O)_2 \cdot H_2O]_n$, where Ln = Gd (**1**) and Nd (**2**) and $Hcit^{3-} = C(OH)(COO^-)(CH_2COO^-)_2$, has been synthesized hydrothermally from Ln_2O_3 and citric acid at 100 °C and characterized by elemental analysis, IR, TG-DTA, single-crystal X-ray diffraction, and magnetic measurements. The structures can be seen as "ladder chains" along the *a* axis, with dinuclear Ln_2O_2 units serving as "steps" and R–COO groups as "uprights", which are connected by H bonds. The magnetic susceptibility between 2 and 300 K and the magnetization at 2 K, as a function of magnetic field between 0 and 5 T, were measured for both compounds. By modeling the magnetic behavior of the Gd compound with a dinuclear Hamiltonian $\mathcal{H}_S = g\mu_B(S_A + S_B)\mathbf{B_o} - J_0 S_A S_B$ ($S_A = S_B = 7/2$), a ferromagnetic exchange interaction $J_0 = 0.039$ cm^{-1} was evaluated between Gd ions situated at $d_0 = 4.321$ Å in dinuclear units bridged by two symmetry-related tridentate carboxylate oxygens. The EPR spectrum of the Gd compound is discussed. The temperature dependence of the susceptibility of the Nd compound is caused by the depopulation of the excited crystal-field levels when the temperature decreases. The magnetic-field dependence of the magnetization of **2** is attributed to the ground-state Kramers' doublet populated at 2 K. The *g* factor of this ground-state doublet is calculated from the data and compared with values for other compounds reported in the literature.

Introduction

The investigation of organic/inorganic hybrid frameworks based on well-defined polydentate carboxylate ligands and lanthanide cations has been a field of rapid growth because of the existence of a large variety of new structures with unique properties, especially in magnetism, luminescence, and catalysis.[1−8] Rare-earth citrates in particular play a predominant role in the Pechini method for the isolation of

* To whom correspondence should be addressed: E-mail: calvo@dfbioq.unl.edu.ar. Fax: +54-342-460-8200 (R.C.). E-mail: perec@q1.fcen.uba.ar. Fax: +54-11-4576-3341 (M.P.).
[†] Comisión Nacional de Energía Atómica.
[‡] Universidad Nacional del Litoral.
[#] Universidad de Chile.
[&] Université de Rennes 1.
[§] Universidad de Buenos Aires.

(1) Reineke, T. M.; Eddaoudi, M.; Moler, D.; O'Keeffe, M.; Yaghi, O. M. *J. Am. Chem. Soc.* **2000**, *122*, 4843.
(2) Lee, E.; Heo, J.; Kim, K. *Angew. Chem., Int. Ed.* **2000**, *39*, 2699.
(3) Mao, J. G.; Zhang, H. J.; Ni, J. Z.; Wang, S. B.; Mak, T. C. W. *Polyhedron* **1999**, *18*, 1519.
(4) Ma, L.; Evans, O. R.; Foxman, B. M.; Lin, W. *Inorg. Chem.* **1999**, *38*, 5837.
(5) Pan, L.; Huang, X.; Li, J.; Wu, Y.; Zheng, N. *Angew. Chem., Int. Ed.* **2000**, *39*, 527.
(6) Reineke, T. M.; Eddaoudi, M.; O'Keeffe, M.; Yaghi, O. M. *Angew. Chem., Int. Ed.* **1999**, *38*, 2590.
(7) Reineke, T. M.; Eddaoudi, M.; Fehr, M.; Kelley, D.; Yaghi, O. M. *J. Am. Chem. Soc.* **1999**, *121*, 1651.
(8) Costes, J. P.; Dahan, F.; Nicodeme, F. *Inorg. Chem.* **2001**, *40*, 5285.

10.1021/ic0510056 CCC: $30.25
Published on Web 10/22/2005

extremely pure multicomponent oxides,[9] as well as for their increasing relevance in biomedical applications.[10] Recently, we reported the first polymeric lanthanum citrate complex $[La(Hcit)(H_2O)]_n$ ($Hcit^{3-}$ = $C(OH)(COO^-)(CH_2COO^-)_2$), whose structure consists of chains of La(III) nodes bridged by O−C−O groups as "linkers" with pendant Hcit anions forming a pillar structure.[11] More recently the isostructural Nd, Eu,[12] and Tb[13] citrates have been reported. All of these were similarly prepared by hydrothermal reactions in the temperature range of 120−170 °C under autogenous pressure, and they crystallize in the monoclinic system, space group $C2/c$.

Because of the multiple denticity of the citrate ligand and the high and variable coordination numbers available to rare-earth cations, it is likely that a variety of structural motifs may be isolated depending on reaction conditions, even if the same molecular blocks are employed. Thus, finding new framework structures with unexpected properties is a main challenge in the area of materials chemistry. With this in mind, hydrothermal synthesis becomes a convenient technique for the preparation of a wide range of organic−inorganic hybrid materials because of the formation of metastable and unique condensed phases, and it may also lead to selective crystallization of products.[14,15]

Since the Gd(III) cation has an $^8S_{7/2}$ ground state without first-order orbital momentum, its compounds are the most suitable for the study of the magnetic properties. As a consequence, investigations of the magnetic properties of many homopolynuclear gadolinium complexes bridged by carboxylate groups, as indicated by the determined X-ray crystal structure, have been reported.[8,16−33] Most of them showed weak antiferromagnetic exchange interactions ($\mathcal{H}_{ex}(i,j) = -J_{ij}\, S_iS_j$) between Gd(III) ions, with coupling constants, J, in the range of −0.05 to −0.43 cm^{-1}.[8,16−22,25−27,31,32] More recently, cases of weak ferromagnetic Gd(III)−Gd(III) interactions transmitted through carboxylate bridges have been reported, with J values in the range of +0.024 to +0.060 cm^{-1}.[23,24,28−31] To clarify and rationalize the physical phenomena underlying the magnetic behavior of dinuclear Gd compounds, more experimental information and analyses are needed. The dual ferromagnetic or antiferromagnetic behavior of the Gd compounds should be further investigated. As reviewed by Benelli and Gatteschi,[34] compounds of lanthanides with unpaired orbital angular momentum are more difficult to model and less information about them exists.

In this paper, we report the hydrothermal synthesis, X-ray crystal structure, and magnetic properties of a novel structural motif for lanthanide citrate complexes, $[Ln(Hcit)(H_2O)_2\cdot H_2O]_n$ (Ln = Gd (**1**), Nd (**2**)). These crystallize in the monoclinic system, $P2_1/n$, with two tridentate carboxylate groups acting as bridges between the two nearest metal centers in the structure. In the case of the Gd compound, we model the susceptibility and magnetization data and evaluate a ferromagnetic-exchange interaction between neighboring Gd(III) ions in dinuclear units. We also provide a qualitative explanation of the observed electron paramagnetic resonance (EPR) spectrum of $[Gd(Hcit)(H_2O)_2\cdot H_2O]_n$, considering the dipolar interactions between Gd(III) ions. In the case of the Nd citrate, we rationalize the susceptibility and magnetization data in terms of the thermal depopulation of the crystal-field levels. The nature of the ground-state Kramers' doublet of the Nd(III) ion is analyzed.

Experimental Section

Materials Preparation. All reagents were commercially available chemicals of analytical or reagent-grade purity and used as received. Water was purified by a Millipore Milli-Q system yielding 18 MΩ cm water. Elemental analyses of C and H were performed on a Carlo Erba 1108 elemental analyzer. Infrared spectra were recorded as KBr pellets and as Nujol mulls on a Nicolet 510P FT-IR spectrophotometer. Thermogravimetric measurements were carried out using a Shimadzu DTG 50 thermal analyzer under an air flow of 40 L/min at a heating rate of 5 °C min^{-1}. The purity of the products was checked by X-ray powder diffraction using

(9) Pechini, M. P. U.S. Patent 3,231,328, 1966. (b) Pechini, M. P. U.S. Patent 3,330,697, 1967. (c) Chandler, C. D.; Roger, C.; Hampden-Smith, M. J. *Chem. Rev.* **1993**, *93*, 1205.
(10) Wang, K.; Li, R.; Cheng, Y.; Zhu, B. *Coord. Chem. Rev*. **1999**, *190*, 297.
(11) Baggio, R.; Perec, M. *Inorg. Chem.* **2004**, *43*, 6965.
(12) Yuan, Y.-Q.; Xu, Y. Q.; Wu, M.-Y.; Hong, M. C. *Acta Crystallogr*. **2005**, *E61*, m108.
(13) Liu, S.-G.; Zuo, W. J.-L.; Li, Y.-Z.; You, X.-Z. *Inorg. Chem. Commun*. **2005**, *8*, 328.
(14) Somiya, S. *Hydrothermal Reactions for Materials Science and Engineering*; Elsevier Applied Science: New York; 1986.
(15) Zubieta, J. In *Comprehensive Coordination Chemistry II*; Elsevier Pergamon: Amsterdam, 2004; Vol. 1, p 579.
(16) Guerriero, P.; Tamburini, S.; Vigato, P. A.; Benelli, C. *Inorg. Chim. Acta* **1991**, *189*, 19.
(17) Liu, S.; Gelmini, L.; Retting, S. J.; Thompson, R. C.; Orvig, C. *J. Am. Chem. Soc*. **1992**, *114*, 6081.
(18) Panagiotopoulus, A.; Zafiropoulos, T. F.; Perlepes, S. P.; Bakalbassis, E.; Masson-Ramade, I.; Kahn, O.; Terzis, A.; Raptopoulou, C. P. *Inorg. Chem.* **1995**, *34*, 4918.
(19) Plass, W.; Fries, G. Z. *Anorg. Allg. Chem*. **1997**, *623*, 1205.
(20) Hedinger, R.; Ghisletta, M.; Hegetschweiler, K.; Tóth, E.; Merbach, A. E.; Sessoli, R.; Gatteschi, D.; Gramlich, V. *Inorg. Chem*. **1998**, *37*, 6698.
(21) Avecilla, F.; Platas-Iglesias, C.; Rodríguez-Cortiñas, R.; Guillemont, G.; Bunzli, J.-C. G.; Brondino, C.; Geraldes, C. F. G. C.; de Blas, A.; Rodríguez-Blas, T. *J. Chem. Soc., Dalton Trans*. **2002**, 4658.
(22) Niu, S. Y.; Jin, J.; Jin, X. L.; Yang, Z. Z. *Solid State Sci.* **2002**, *4*, 1103.
(23) Costes, J.-P.; Clemente-Juan, J. M.; Dahan, F.; Nicodéme, F.; Verelst, M. *Angew. Chem., Int. Ed.* **2002**, *41*, 323.
(24) Hou, H.; Li, G.; Li, L.; Zhu, Y.; Meng, X.; Fan, Y. *Inorg. Chem*. **2003**, *42*, 428.
(25) Nishihara, S.; Akutagawa, T.; Hasegawa, T.; Nakamura, T. *Inorg. Chem*. **2003**, *42*, 2480.
(26) Wai-Hing Lam, A.; Wong W.-T.; Gao S.; Wen G.; Zhang X.-X. *Eur. J. Inorg. Chem*. **2003**, 149.
(27) Rizzi, A.; Baggio, R.; Garland, M. T.; Peña, O.; Perec, M. *Inorg. Chim. Acta* **2003**, *353*, 315.
(28) Hatscher, S. T.; Urland, W. *Angew. Chem., Int. Ed*. **2003**, *42*, 2862. See, also: Favas, M. C.; Kepert, D. L.; Skelton, B. W.; White, A. H. *J. Chem. Soc., Dalton Trans*. **1980**, 454.
(29) Costes, J.-P.; Clemente-Juan, J.-M.; Dahan, F.; Nicodéme, F. *Dalton Trans.* **2003**, 1272.
(30) Hernandez-Molina, M.; Ruiz-Perez, C.; Lopez, T.; Lloret, F.; Julve, M. *Inorg. Chem*. **2003**, *42*, 5456.
(31) Rohde, A.; Hatscher, S. T.; Urland, W. *J. Alloys Compd*. **2004**, 374, 137.
(32) Atria, A. M.; Baggio, R.; Garland, M. T.; Muñoz, J. C.; Peña, O. *Inorg. Chim. Acta* **2004**, *357*, 1997.
(33) He, Z.; Gao, E.-Q.; Wang, Z.-M.; Yan, C.-H.; Kurmoo, M. *Inorg. Chem*. **2005**, *44*, 862.
(34) Benelli, C.; Gatteschi, D. *Chem. Rev.* **2002**, *102*, 2369.

monochromated Cu Kα radiation on a Phillips X'Pert diffractometer.

Syntheses of $[Gd(C_6H_5O_7)(H_2O)_2.H_2O]_n$ (1) and $[Nd(C_6H_5O_7)(H_2O)_2.H_2O]_n$ (2). A mixture of Ln_2O_3 (Ln = Gd, Nd; 1 mmol), citric acid monohydrate (0.25 g, 1 mmol), and water (20 mL), was placed in a Parr Teflon-lined stainless-steel vessel (45 cm^3), and the vessel was sealed and heated at 100 °C for 10 days. After it was cooled at a rate of 0.5 °C min^{-1}, colorless crystals of **1** and **2** were collected (the yield in both cases was about 75% based on Ln_2O_3). The pH of the remaining solution was 2.5. The crystalline materials were washed with deionized cold water and dried under vacuum. Anal. Calcd for complex **1**, $C_6H_{11}GdO_{10}$: C, 17.98; H, 2.75. Found: C, 18.05; H, 2.80. Anal. Calcd for complex **2**, $C_6H_{11}NdO_{10}$: C, 18.58; H, 2.86. Found: C, 19.05; H, 2.90. Optical examination, combined with X-ray powder diffraction, indicated phase purity for both cases. Once isolated, compounds **1** and **2** are insoluble in most common polar and nonpolar solvents.

Main FT-IR bands (KBr pellet, cm^{-1}) for compound **1**: ν 3595 m, 3406 m, 3402 m, 1573 vs, $\nu(CO_2^-)_{asym}$, 1505 s, 1403 vs, 1303 s, 1400s, $(\nu(CO_2^-)_{sym}$, 1303 s, 1264 vs, 1188 s, 1139 m, 1076 s, 946 w, 905 w, 865 w, 761 w, 728 m, 674 s, 557 s, 540 s, 490 m, 440 w. The IR spectrum for compound **2** is similar to that of complex **1** within ± 5 cm^{-1}. Thermogravimetric analysis exhibited losses corresponding to one water molecule below 100 °C and two water molecules per formula unit in the range of 130−250 °C. These contributions should correspond to the hydration molecule and to the two coordinated water molecules per formula unit, respectively. The final residual mass at 800 °C (65% approximately) corresponds to the formation of Gd_2O_3 for complex **1** and Nd_2O_3 for complex **2**, as confirmed by XRD**.**

Magnetic and EPR Measurements. Susceptibility and magnetization measurements were performed in powder samples with a Quantum Design SQUID magnetometer model MPMS XL5, using calibrated gelatin capsules as sample holders with a small diamagnetic contribution. The magnetic susceptibility was measured in the temperature interval between 2 and 300 K, with an applied field of 25 mT. The magnetization measurements were performed at 2 K, with a maximum field of 5 T.

The diamagnetic contribution to the susceptibility and magnetization of **1** and **2** are small compared with the paramagnetic contribution of the high-spin Gd(III) and Nd(III) ions; the values of the susceptibility and magnetization of **1** and **2** presented below were corrected for the diamagnetism of the constituent atoms using a value of -142×10^{-6} cm^3 mol^{-1} per Ln unit, obtained using Pascal's constants.[35−37] The contribution of the gelatin capsules was subtracted from the measured values.

The EPR measurements of powdered samples of La,[11] Gd, and Nd citrates were performed at room temperature with a Bruker ER200 X-band spectrometer, using a cylindrical cavity with 100 kHz field modulation. As expected, only signals of the Gd compound were observed. EPR spectra were simulated using Easyspin 2.1.1.[38]

X-ray Crystallography. Single-crystal X-ray measurements of **1** and **2** were performed at room temperature on a Bruker SMART CCD diffractometer, with graphite monochromated Mo Kα radiation. The structures were primarily solved by direct methods and completed by difference Fourier synthesis. Refinement of the models was performed by the least-squares method on F^2 with anisotropic displacement factors for non-H atoms. C−H hydrogen atoms were idealized at their expected positions (C−H = 0.97 Å) and allowed to ride; O−H hydrogens were found in a late difference Fourier synthesis and refined with a restrained O−H (0.85(1) Å) distance. All hydrogen atoms were assigned isotropic displacement factors 1.2 times larger than those of the parent atom to which they were attached. All calculations to solve and refine the structures and to obtain derived results were carried out with the computer programs SHELXS 97, SHELXL 97, and SHELXTL/PC.[39]

Full use of the CCDC package was made using the CSD Database.[40] Crystallographic data and other pertinent information for **1** and **2** are summarized in Table 1. Selected bond distances and bond angles are listed in Table 2. More details on the crystallographic studies as well as atomic displacement parameters are given as Supporting Information in a CIF file.

Table 1. Crystal Data and Structure Refinement for 1 and 2[a]

	1	**2**
empirical formula	$C_6H_{11}GdO_{10}$	$C_6H_{11}NdO_{10}$
fw	400.40	387.39
temp (K)	298(2)	298(2)
λ(Mo Kα) (Å)	0.71073	0.71073
cryst syst	monoclinic	monoclinic
space group	$P2_1/n$	$P2_1/n$
a (Å)	6.1448(8)	6.2296(5)
b (Å)	9.6536(12)	9.7066(8)
c (Å)	16.946(2)	17.0175(14)
β (deg)	92.170(2)	91.3170(10)
V (Å^3)	1004.5(2)	1028.75(15)
Z	4	4
density$_{calcd}$ (g cm^{-3})	2.648	2.501
F(000)	764	748
abs coeff (mm^{-1})	6.650	5.094
cryst size (mm^3)	0.25 × 0.08 × 0.06	0.22 × 0.06 × 0.06
min/max transmission	0.53, 0.67	
θ range (deg)	2.41 to 27.99	
index ranges	$-8 \le h \le 8$	$-8 \le h \le 8$
	$-12 \le k \le 12$	$-12 \le k \le 12$
	$-22 \le l \le 20$	$-21 \le l \le 21$
N_{tot} N_{uniq}(R_{int})	8192	8387
$N_{[I>2\sigma(I)]}$	2262(0.0456)	2363(0.0264)
	1887	2163
params refined	186	186
GOF on F^2	1.207	1.045
final R indices [$I>2\sigma(I)$]	R1 = 0.0358[a]	R1 = 0.0229[a]
	wR2 = 0.0768[b]	wR2 = 0.0768[b]
R indices (all data)	R1 = 0.0447[a]	R1 = 0.0546[a]
	wR2 = 0.0799[b]	wR2 = 0.0559[b]
ρ_{max}/ρ_{min} in final ΔF(eÅ^{-3})	1.036 and −2.009	0.828 and −0.506

[a] $R1 = \sum||F_o| - |F_c||/\sum|F_o|$. [b] $wR2 = \{\sum[w(F_o^2 - F_c^2)^2]/\sum[w(F_o^2)^2]\}^{1/2}$.

Results and Discussion

Crystal Structures. Compounds 1 and 2 are isostructural and crystallize in the monoclinic space group $P2_1/n$ as linear polymers. Figure 1shows a schematic representation of **1** with only the independent unit drawn in full ellipsoids. Because the ionic radius of Nd(III) is slightly larger than that of the Gd(III) ion, all metal−ligand bonds in **2** are larger than the corresponding bonds in **1**, see Table 2. However, the bond angles are nearly the same for **1** and **2** (see Supplementary Information).

(35) Pascal, P. *Ann. Chim. Phys*. **1910**, *19*, 5.
(36) Carlin, R. *Magnetochemistry*; Springer: Berlin, 1986.
(37) Kahn, O. *Molecular Magnetism*; Wiley VCH: New York, 1993.
(38) Stoll, S. Spectral Simulations in Solid-State EPR. Ph.D. Thesis, ETH, Zürich, 2003. (b) *IES EPR Newsl*. **2003**, *13*, 22. (c) Program available at http://www.esr.ethz.ch/EasySpin/home.html
(39) Sheldrick, G. M. *SHELXS-97*, *SHELXL-97*, and *SHELXTL/PC*: *Programs for solution and refinement of crystal structures*; University of Göttingen: Göttingen, Germany, 1997.
(40) Allen, F. H. *Acta Crystallogr*. **2002**, *B58*, 380. (b) Orpen, A. G. *Acta Crystallogr*. **2002**, *B58*, 398.

Table 2. Selected Bond Distances (Å) and Angles (deg) for **1** and **2**[a]

	1	**2**
Ln(1)−O(3)	2.381(5)	2.435(3)
Ln(1)−O(7)#1	2.387(4)	2.449(2)
Ln(1)−O(2W)	2.428(5)	2.501(3)
Ln(1)−O(1W)	2.415(5)	2.461(2)
Ln(1)−O(5)	2.413(4)	2.461(2)
Ln(1)−O(4)	2.435(4)	2.485(2)
Ln(1)−O(2)#2	2.508(4)	2.556(2)
Ln(1)−O(2)#1	2.521(4)	2.551(2)
Ln(1)−O(1)#2	2.591(4)	2.625(2)
Ln(1)···Ln(1)#3	4.321(4)	4.389(2)
Ln(1)···Ln(1)#4	6.145(4)	6.230(2)
Ln(1)···Ln(1)#2	6.383(4)	6.413(2)
O(2)#4−Ln(1)−O(2)#2	61.5(2)	61.5(1)

[a] Symmetry transformations used to generate equivalent atoms: #1 $x + 1, y, z$; #2 $-x + 1, -y, -z + 2$; #3 $-x + 2, -y, -z + 2$; #4 $x - 1, y, z$.

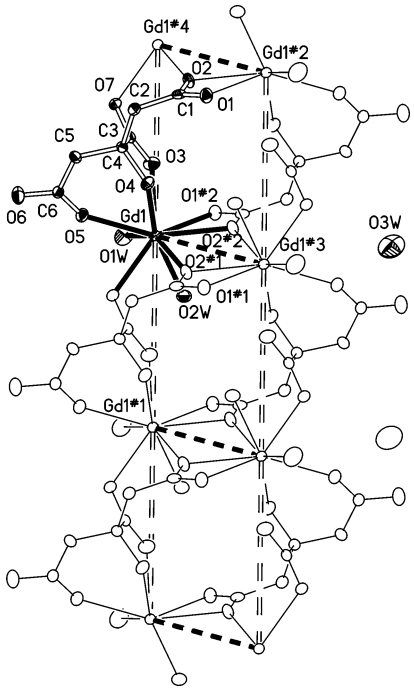

Figure 1. Molecular structure and schematic representation of a ladder chain. Only the independent unit has been drawn in full ellipsoids. Symmetry codes: #1 $x + 1, y, z$; #2 $-x + 1, -y, -z + 2$; #3 $-x + 2, -y, -z + 2$; #4 $x - 1, y, z$. The ladder steps have been suggested in full broken lines and the [100] uprights in double broken lines.

The citrate anion coordinates through six out of its seven possible donor oxygens (O6 being the exception). Five of them act in a simple mode; only O2 binds in a bifurcated or bridging fashion. The presence of two aqua molecules completes a rather even O9 coordination environment, with Gd−O bond distances in the range 2.381(4)−2.591(4) Å for **1** and Nd−O bonds in the range 2.435(3)−2.625(2) Å for **2**. For comparison purposes, a search in the Cambridge Structural Database[40] looking for similar GdO_9/NdO_9 environments gave 83/156 cases with mean Ln−O values of 2.448(85)/2.561(82) Å, respectively.

Besides binding to the reference cation Gd1 in Figure 1 through O3, O4, and O5, the anion links to the metallic centers Gd1#2 at $(1 - x, -y, 2 - z)$ via O1 and O2 and to Gd1#4 at $(-1 + x, y, z)$ via O2 and O7. The Gd coordination polyhedra thus formed interact with each other in an intricate fashion to form chains which run along *a*. The connectivity between cations is achieved via three types of well-differentiated closed loops. The first one is around the inversion symmetry center at (1,0,1), with O2 as the sole bridging agent linking cations Gd1 and Gd1#3 to a short distance of 4.321(4) Å. The second is non-centrosymmetric, it evolves along the *a* axis with two different bridges, a short one, Gd1−O3−C3−O7−Gd1#4, and a much longer one, Gd1−O4−C4−C2−C1−O2−Gd1#4, leading to the second-nearest intercationic approach Gd1···Gd1#4 of 6.145(4) Å. The third one is around the nonequivalent symmetry center at (0.5, 0, 1) and through a much longer pathway (Gd1−O4−C4−C2−C1−(O2/O1)−Gd1#2 and back) leading to a Gd1···Gd1#2 distance of 6.383(4) Å. For compound **2**, the distances corresponding to these pathways are 4.389(2), 6.230(2), and 6.413(2) Å, respectively. We consider that the first pathway described above, containing two symmetry-related carboxylate oxygens (O2), supports the strongest exchange interactions between Gd ions. In the magnetic analysis that follows, we ignore the third pathway, which contains five diamagnetic atoms, instead of one or three as in the first and second described pathways. The contribution of the second pathway will be discussed further. The noticeable differences between the first and second neighbor Gd···Gd distances give the linear array the "ladderlike" appearance shown in Figure 1 for compound **1**, where the "steps" have been suggested in heavy broken lines and the [100] "uprights" in weak double broken lines. The interlinking of the chains is achieved through H bonding only (see Table 3), to which the two aqua and the hydration water molecules provide five donor hydrogens, all of them clearly detectable in the difference Fourier maps. The sixth hydrogen, attached to O3W, does not seem to be involved in any such interaction.

This eminently 1D arrangement for **1** and **2** contrasts with the packing found in the previously reported series, $[Ln(Hcit)(H_2O)]_n$ (La, Nd, Eu, and Tb), where chains are bound together by sharing covalent bonds with the citrate ligands, as well as by H bonds, leading to compact 3D structures.[11−13] The two packing schemes, viewed down the chains, are compared in Figure 2.

Magnetic Properties and EPR. The molar susceptibilities χ_m of both compounds measured at temperatures (*T*) between 2 and 300 K are plotted in Figures 3a and 4a for compounds 1 and 2, respectively, as[41]

$$\frac{\mu_{eff}}{\mu_B} = (3k_B/\mu_o N)^{1/2}(\chi_m T)^{1/2} \quad (1)$$

In the high *T* limit, $\mu_{eff}^2/\mu_B^2 \approx g^2 S(S + 1)$. For compound **1**, the μ_{eff} value of $\sim$7.92 μ_B observed near room temperature indicates that $g \approx 1.99$, a typical *g* value for Gd(III) $^8S_{7/2}$ ions. At 20 K, $\mu_{eff} \approx 7.97$ μ_B, and it rapidly increases at lower temperatures, reaching $\mu_{eff} \approx 8.65$ μ_B at 2 K (Figure 3a), indicating predominant ferromagnetic interactions between Gd(III) ions. The susceptibility data for compound **2**

(41) Hatscher, S.; Schilder, H.; Lueken, H.; Urland, W. *Pure Appl. Chem.* **2005**, *77*, 497.

Table 3. Hydrogen Bonds (Å and deg) for **1** and **2**[a]

	d(D−H)		*d*(H···A)		*d*(D···A)		∠(DHA)	
D−H···A	**1**	**2**	**1**	**2**	**1**	**2**	**1**	**2**
O(4)−H(4)···O(6)#5	0.85(1)	0.84 (1)	1.69(2)	1.71(2)	2.524(6)	2.533(4)	169(11)	165(5)
O(1W)−H(1WA)···O(3W)#6	0.85 (1)	0.85(1)	1.88(3)	1.88(2)	2.710(9)	2.722(5)	165(12)	170(6)
O(1W)−H(1WB)···O(2W)#7	0.85 (1)	0.85(1)	2.41(14)	2.13(3)	2.913(7)	2.854(4)	119(12)	143(4)
O(2W)−H(2WA)···O(6)#8	0.85 (1)	0.85(1)	1.81(2)	1.83(2)	2.652(7)	2.665(4)	169(9)	167(6)
O(2W)−H(2WB)···O(3)#1	0.85 (1)	0.85(1)	1.91(4)	1.88(2)	2.684(6)	2.691(4)	151(7)	159(5)
O(3W)−H(3WA)···O(1)#2	0.86(1)	0.86(1)	2.16(6)	2.05(2)	2.838(8)	2.853(4)	135(7)	156(5)

[a] Symmetry transformations used to generate equivalent atoms: #1 $x+1, y, z$; #2 $-x+1, -y, -z+2$; #3 $-x+2, -y, -z+2$; #4 $x-1, y, z$; #5 $-x+3/2, y-1/2, -z+3/2$; #6 $-x+1, -y+1, -z+2$; #7 $-x+2, -y+1, -z+2$; #8 $x+1/2, -y+1/2, z+1/2$.

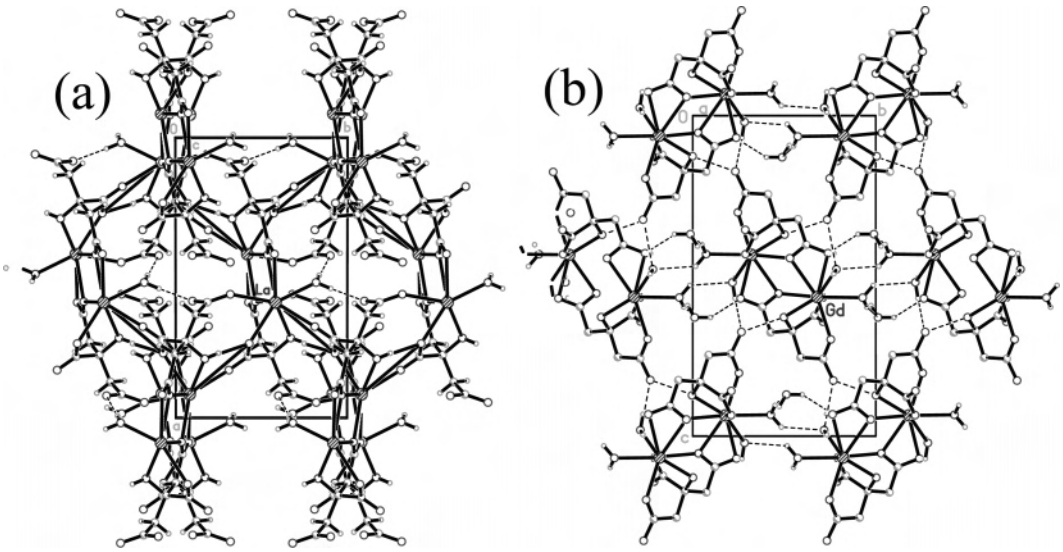

Figure 2. Comparative packing views along the polymeric chain axis for (a) 3D $[La(Hcit)(H_2O)]_n$[11] and (b) 1D $[Gd(Hcit)(H_2O)_2 \cdot H_2O]_n$.

(Figure 4a) show that $\mu_{eff} \approx 3.37\ \mu_B$ at 300 K, and it decreases monotonically with decreasing temperature to $\mu_{eff} \approx 2.19\ \mu_B$ at 2 K. The value of μ_{eff} observed at 300 K is already smaller than the value $\mu_{eff} = 3.45\ \mu_B$ expected for free Nd(III) ions having a $^4I_{9/2}$ ground multiplet.[36] This value and the reduction of μ_{eff} at lower T are clearly related to the thermal depopulation of the crystal-field energy levels of the multiplet.

The magnetization as a function of the applied magnetic field $\mathbf{B_o} = \mu_o \mathbf{H}$ at $T = 2$ K for $\mathbf{B_o}$ between 0 and 5 T, is displayed in Figures 3b and 4b in units of Bohr magnetons (μ_B)/Ln atom for compounds **1** and **2**, respectively. The magnetization of the Gd compound reaches almost complete saturation for a field of 5 T. Meanwhile that of the Nd compound still increases at this magnetic field, supporting the depopulation of excited-crystal field states when the temperature is lowered.

We modeled the magnetic behavior of **1** and **2** to evaluate the exchange interactions between Ln ions from the magnetic data (Figures 3 and 4). This is possible for the Gd(III) compound, but it is more complicated for the Nd(III) compound, which has orbital degeneracy and large crystal-field splittings.[34]

For the three-dimensional arrangement of the Ln(III) ions (Figure 1) described above, we call J_o the magnitude of the exchange interaction within the Gd_2O_2 dinuclear units and J_1 that between the Gd ions connected by the carboxylate bridges O3−C3−O7. Abundant literature exists about ladder chains with spins of $S = 1/2$, which are important in the theory of high-temperature superconductors.[42] However, we did not find information about quantum ladder chains of spins of 7/2, where the theoretical analysis is more difficult. Also, classical approaches,[43] used to analyze data for uniform Gd spin chains,[29] have not been treated for the more complex ladder chains.

Exchange interactions between Gd ions are expected to decrease exponentially with distance,[44,45] so it is reasonable to assume that $|J_1| \ll |J_o|$ because of the longer distance (6.145 Å vs 4.321 Å) and higher complexity of the O3−C3−O7 carboxylate connections (J_1) compared to the pathway with two symmetry-related oxygens O2 (J_o). In this analysis, we neglect all exchange interactions between nearest-neighbor Gd ions, except J_o. These approximations are not valid for the series of lanthanide citrates (La, Nd, Eu, Tb) studied previously,[11−13] with zigzag chains with two nearest lanthanide neighbors at nonnegligible distances.

At the temperature of the experiments, because of anisotropy, the contributions of dipole−dipole interactions to magnetic susceptibility and magnetization of powder samples are averaged out.[36] Also, the role of the zero-field splitting is expected not to be important because of both its small

(42) Dagotto, E.; Rice, T. M. *Science* **1996**, *271*, 618.
(43) Fisher, M. E. *Am. J. Phys.* **1964**, *32*, 343.
(44) Coffman, R. E.; Buettner, G. R. *J. Phys. Chem.* **1979**, *83*, 2387.
(45) Hoffmann, S. K.; Hilczer, W.; Goslar, J. *Appl. Magn. Reson.* **1994**, *7*, 289.

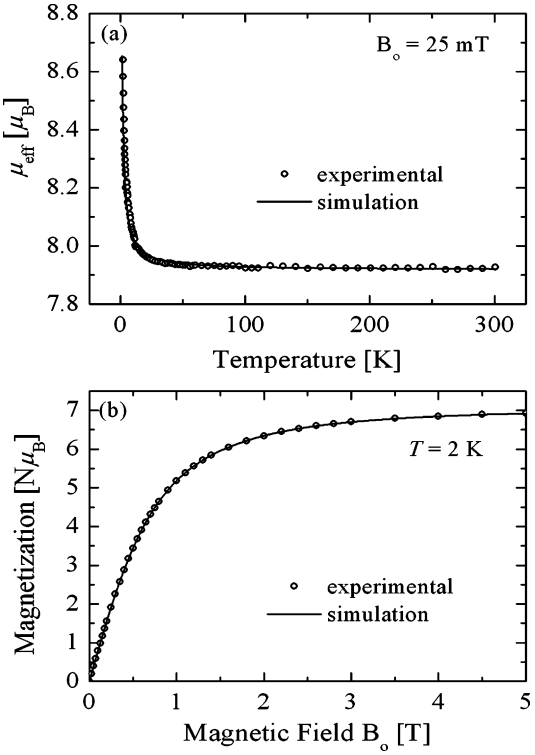

Figure 3. (a) Thermal variation of μ_{eff} for compound **1**; μ_{eff} increases at low temperatures as expected for a system with ferromagnetic interactions. (b) Magnetic-field dependence of the molar magnetization of Gd(III) citrate observed at 2 K. The solid lines in panels a and b are obtained from a global fit of eq 2 to the susceptibility and magnetization data, giving g = 1.995 and J_o = 0.039 cm^{-1}.

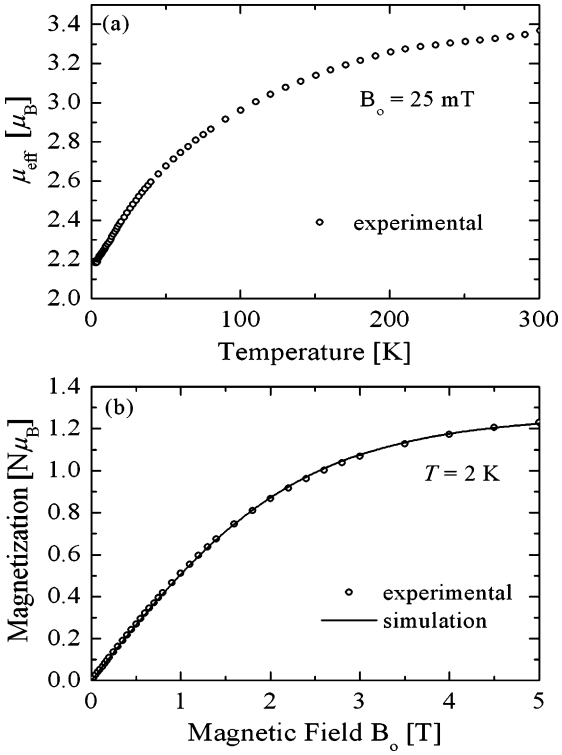

Figure 4. (a) Thermal variation of μ_{eff} for compound **2**. The observed temperature variation of μ_{eff} is a consequence of the depopulation of the higher crystal-field levels when the temperature is lowered. (b) Magnetic-field dependence of the molar magnetization of Nd(III) citrate. The solid line is obtained from a fit assuming that at 2 K only the ground-state Kramers' doublet contributes to the magnetization.

magnitude and the anisotropy averaging out a large part of the contribution. To evaluate g and J_o, we analyzed the magnetic data for the Gd compound using the simple dinuclear Hamiltonian

$$\mathscr{H}_S = g\mu_B(S_A + S_B)\cdot\mathbf{B_o} - J_oS_A\cdot S_B \qquad (2)$$

where S_A and S_B are the spins of the two Gd(III) (S = 7/2) in a dinuclear unit and g is the isotropic g factor expected for the S-state Gd ions. The molar magnetization of the Gd compound as a function of T and $\mathbf{B_o}$ was calculated using eq 2 and

$$M(\mathbf{B_o},T) = -Ng\mu_B\frac{Tr[S_z\exp(-\mathscr{H}_S/k_BT)]}{Z} \qquad (3)$$

where Tr represents the trace of the operator in parentheses, S_z is the z component of the angular momentum of the states, and Z is the partition function defined as

$$Z = Tr[\exp(-\mathscr{H}_S/k_BT)]$$

Since the susceptibility measurements were performed at low magnetic field (25 mT), the susceptibility χ_m was calculated by dividing $M(\mathbf{B_o},T)$ by $\mathbf{B}_o$ and μ_{eff} was calculated using eq 1.

The parameters g and J_o for 1 were obtained from a global fit of eqs 1, 2, and 3 to the experimental values of the effective magnetic moment $\mu_{eff}(T)$ and magnetization $M(\mathbf{B_o},T)$ displayed in Figure 3a and b, using eqs 1−3. We calculated the standard deviations σ_μ and σ_M of μ_{eff} and M, separately, for a wide range of values of the parameters g and J_o. A normalized global standard deviation, σ_g, was obtained adding the contributions σ_μ and σ_M, each divided by the mean value of the property in the fitted interval. The smallest σ_g was obtained for g = 1.995(5) and J_o = 0.039(4) cm^{-1}. It is noteworthy that the dinuclear model of eqs 2 and 3 gives a better fit to the magnetization data than that obtained applying the Brillouin function for uncoupled S = 7/2 Gd(III) spins. The agreement between the data and the calculated curves $\mu_{eff}(T)$ and $M(\mathbf{B}_o)$ is well within the experimental errors (see solid lines in Figure 3a and b), supporting the adequacy of the dinuclear model neglecting the exchange interaction J_1 between next-nearest Gd neighbor ions in the uprights of the ladders. The model also neglects anisotropic zero-field splitting of the Gd(III) ions and dipolar interactions between them, which are mostly averaged out in the powder. We also verified that the values of $\mu_{eff}(T)$ and $M(\mathbf{B}_o)$ calculated considering dipolar interaction within dinuclear units differ by less than 0.2% from those neglecting interactions, justifying the use of eq 2 in the experimental range of temperature.

The magnetic properties of the Nd sample displayed in Figure 4a and b are determined by the crystal-field splitting into five Kramers' doublets within an energy span of few hundred units (cm^{-1}), expected for the $^4I_{9/2}$ ground term of the Nd(III) ion in a low-symmetry environment.[46−48] At 2

(46) Gruber, J. B.; Satten, R. A. *J. Chem. Phys.* **1963**, *39*, 1455.

K, where the magnetization measurements were performed, one should expect only ground-state doublet contributions. Thus, the magnetization curve of Figure 4b is the result of population changes within the ground-state doublet, split by the magnetic field. Accordingly, we modeled the magnetization data for the powder sample of compound **2** as coming from an effective spin, S_{eff}, of 1/2 with an effective angular average of the anisotropic g factor, g_{eff}, expected for a ground-doublet state in a low-symmetry environment. To determine this parameter, a single-crystal EPR experiment at low T would be necessary.[48−51] A least-squares fit gives $g_{eff} = 2.52$, and the calculated magnetization curve (solid line in Figure 4b) is in very good agreement with the experimental data. No further improvement of the fit is obtained by introducing exchange interactions between effective spins within the dinuclear unit. In comparison, single-crystal EPR measurements reported by Bleaney et al.[49] for Nd(III) impurities in La ethylsulfate gave an average value of $g = 2.56$ for the ground-state doublet, and Hutchison and Wong[50] and Halford[51] reported an average value of 2.51 for Nd(III) impurities in $LaCl_3$. Our result, $g_{eff} = 2.52$, is similar to these values.

The magnetic susceptibility data displayed in Figure 4a is the result of the depopulation of the excited crystal-field levels when the temperature is decreased and could be explained if optical spectroscopy information would be available for compound **2**. As an example, Gruber and Satten[46] found that the two first-excited Kramers' doublets are at 149 and 154 cm^{-1} for Nd(III) in La ethylsulfate and, Eisenstein[47] found that these doublets are at 115 and 123 cm^{-1} for Nd(III) in $LaCl_3$. Similar values would be expected for compound **2**.

The EPR spectrum of a powder sample of compound **1** is shown in Figure 5. The dinuclear model of eq 2 explains the susceptibility and magnetization data, yet a more sophisticated model is needed to explain its EPR spectra.[52,53] This is because the magnetic parameters are an average over field orientations but the EPR spectrum is a convolution over field orientations. Also, in eq 2, the Heisenberg isotropic-exchange interaction term commutes with the Zeeman term and the EPR spectrum of a dinuclear unit with identical and isotropic g factors and no zero-field splitting or magnetic-dipolar interactions would be identical to that obtained for a single spin. However, the spectrum strongly depends on dipolar interactions except when exchange interactions are very large, and exchange narrowing processes appear.[54] Dipolar interactions and zero-field splittings shift the resonance signal as a consequence of magnetic-field orientation, producing

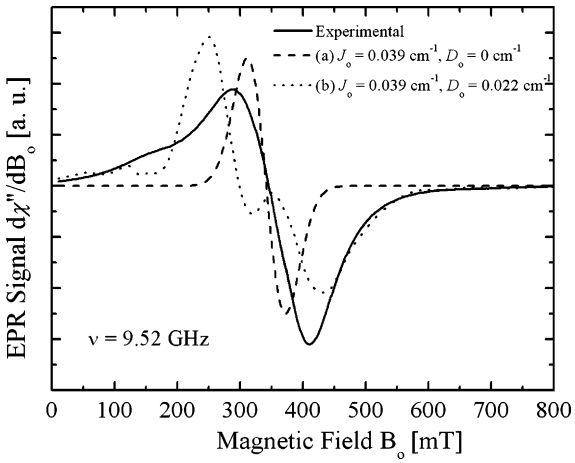

Figure 5. Room-temperature EPR spectrum of Gd(III) citrate. The solid line is the experimental result. The dashed line is a simulation assuming that only exchange and Zeeman interactions (eq 2) contribute. The dotted line is a simulation that also considers the dipolar interaction within the dinuclear unit.

deformations, broadening, and structure of the spectrum, as observed in Figure 5. The dipolar interactions between two spins i and j at a distance d, connected by a unit vector $\hat{\mathbf{r}}$, can be written under the point-dipole approximation as

$$\mathscr{H}_{dip}(i,j) = \frac{\boldsymbol{\mu}_i \cdot \boldsymbol{\mu}_j}{d^3} - 3\frac{(\boldsymbol{\mu}_i \cdot \hat{\mathbf{r}})(\boldsymbol{\mu}_j \cdot \hat{\mathbf{r}})}{d^3} = \frac{g^2 \mu_B{}^2}{d^3}[\mathbf{S}_i \cdot \mathbf{S}_j - (\mathbf{S}_i \cdot \hat{\mathbf{r}})(\mathbf{S}_j \cdot \hat{\mathbf{r}})] \quad (4)$$

where $D_o = g^2\mu_B{}^2/d_o{}^3 = 0.022$ cm^{-1} and $D_1 = g^2\mu_B{}^2/d_1{}^3 = 0.008$ cm^{-1} for the nearest- and next-nearest-neighbor Gd pairs, respectively, both having the same orders of magnitude of the expected exchange interactions. Further, because of the weak distance dependence (d^{-3}) of the dipolar interactions and the growing number of Gd(III) neighbors at longer distances (increasing proportionally to d^2), a wide distribution of magnitudes and orientations of the dipolar interactions between one Gd ion and neighboring Gd ions in the same and in other ladders are expected to contribute to the spectrum. Considering only the dipolar interactions between S_A and S_B within the dinuclear unit, we added the dipolar interaction to eq 2

$$\mathscr{H}_{dip} = \frac{\boldsymbol{\mu}_A \cdot \boldsymbol{\mu}_B}{d_o{}^3} - 3\frac{(\boldsymbol{\mu}_A \cdot \hat{\mathbf{r}})(\boldsymbol{\mu}_B \cdot \hat{\mathbf{r}})}{d_o{}^3} = D_o[S_{Ax}S_{Bx} + S_{Ay}S_{By} - 2S_{Az}S_{Bz}] \quad (5)$$

which assumes that S_A and S_B are along the $\boldsymbol{z}$ direction (this is irrelevant in the final result because the g factor is isotropic). The next approximation to the problem would be to consider the dipolar interactions of one dinuclear unit with the two neighboring dinuclear units in a ladder chain. Considering the contribution of the zero-field splitting of Gd(III) ions would introduce several new experimental parameters and could be done only in cases where single-crystal EPR data were available.

Together with the observed EPR spectrum (solid line), we include in Figure 5 two simulations obtained with Easyspin[38]

(47) Eisenstein, J. C. *J. Chem. Phys*. **1963**, *39*, 2134.
(48) Abragam, A.; Bleaney, B. *Electron Paramagnetic Resonance of Transition Ions*; Clarendon Press: Oxford, 1970.
(49) Bleaney, B.; Scovil, H. E. D.; Trenam, R. S. *Proc. R. Soc. London* **1954**, *A223*, 15.
(50) Hutchison, C. A.; Wong, E. *J. Chem. Phys*. **1958**, *29*, 754.
(51) Halford, D. *Phys. Rev*. **1962**, *127*, 1940.
(52) Bencini, A.; Gatteschi. D. *Electron Paramagnetic Resonance of Exchange Coupled Systems*; Springer: Berlin, 1990.
(53) Weil, J. A.; Bolton, J. R.; Wertz, J. E. *Electron Paramagnetic Resonance. Elementary Theory and Practical Applications*; Wiley: New York, 1994.
(54) Anderson, P. W. *J. Phys. Soc. Jpn.* **1954**, *9*, 316.

Table 4. Magnetostructural Information about Ferromagnetic and Antiferromagnetic Bridges Connecting Gd(III) Ions[a]

compound	J_o (cm^{-1})	bridge topology[b]	angle Gd−O−Gd (deg)	Gd−Gd distance (Å)	ref
a $[Gd(Hcit)(H_2O)_2 \cdot H_2O]_n$	0.039	A	118.49	4.321	this work
b $[Gd(AcO)_3(H_2O)_2] \cdot 4H_2O$	0.060	A	115.48	4.206	28
c $[Gd_2(L^1)_3(H_2O)_6]_n$	0.048	A	116.71	4.276	30
d $[Gd(L^2)(H_2O)(SO_4)]_n$	0.024	A[c]	113.64	4.143	31
e $[Gd_2BzO)_6(phen)_2]$	−0.430	B	101.47	4.053	22
f $[Gd_2(L^3)_6(phen)_2]$	AFM[d]	B	104.94	3.937	27
g $[Gd_2(L^3)_6(H_2O)_4] \cdot 4bpa$	AFM[d]	B	105.64	3.992	32
h $[Gd_2(L^3)_6(bipy)_2]$	AFM[d]	B	106.08	3.936	32
i $[Gd(H_2L^4(HL^4)(L^4)(H_2O)]_n$	0.037	C	111.85−114.29	4.187	29

[a] L^1 = 1,3-propanedioic (2−), L^2 = isonicotinate-*N*-oxide (1−), HL^3 = *trans*-2-butenoic acid, HL^4 = salicylic acid. Compounds with unknown X-ray structures[18,23] or 3d metal ions[24,25] are not included. [b] Bridging motifs A and B are centrosymmetric. C is noncentrosymmetric. [c] The two O bridges in the Gd_2O_2 core belong to sulfate groups. [d] Reported to be antiferromagnetic (AFM), but the value of J_o was not calculated.

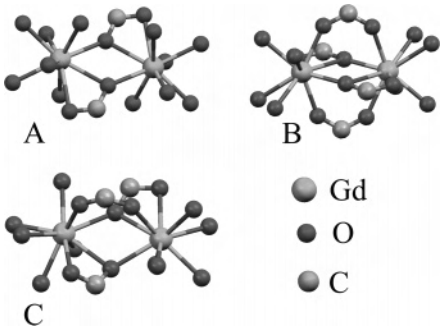

Figure 6. Chemical bridges supporting exchange interactions between Gd(III) ions in homodinuclear units reported to be ferromagnetic (A and C) and antiferromagnetic (B).

in the cases where (a) only the *g* factor and the exchange interaction J_o evaluated from the magnetic data are considered (eq 2) (dashed line) and (b) dipolar interactions between nearest neighbor Gd(III) ions are introduced, as calculated from the structural data (eq 5) (dotted line). The same intrinsic line width is assumed in a and b. As explained above, case a produces the narrow spectrum expected for uncoupled Gd(III) ions without zero-field splitting. Case b gives a structured broader spectrum, closer to the experimental result, but with extra central splittings. The next approximation to the simulation would be a molecule containing 6 Gd atoms, corresponding to three neighbor dinuclear units in a chain with additional dipolar couplings with magnitudes $D_1 = 0.008$ cm^{-1} and different sets of axes (Figure 1). Six Gd (7/2) spins would represent a quantum system with $8^6 = 262144$ states, hard to analyze even with large computers. However, it is reasonable to assume that the dipolar interactions between Gd neighbors along the uprights of the ladders would average out the features of the central part of the spectrum simulated considering only exchange and dipolar interactions within a dinuclear unit. In addition, since dipolar interactions decrease in magnitude as d^{-3} and the number of interacting neighbors increases as d^2, simulated spectra obtained considering Gd neighbors at longer distances would approach the experimental spectrum.

In the previous discussion, we did not consider zero-field splitting terms. We do not mean that they should be neglected, yet we consider that for this system the main features of the observed powder spectrum can be well explained by only assuming dipolar interactions between Gd ions. According to early results of Bleaney et al.,[49] for Gd(III) ions magnetically diluted in Lanthanum ethylsulfate, where the Ln ions are surrounded by 9 water oxygens, there is a maximum splitting of ±124 mT of the outermost peaks $\pm 5/2 \leftrightarrow \pm 7/2$. Since splittings within these magnitudes are not observed in the experimental spectrum, we suggest that the corresponding values for **1** are probably smaller. Indeed, a reduction of the zero-field splitting is expected because of the spin dynamics introduced by the exchange interactions. A single-crystal EPR study would be needed to analyze this problem in more detail. This was not possible in the present work because the available single crystals of Gd citrate were too small.

The value of J_o obtained for compound **1** can be compared with the values observed for related complexes containing similar dinuclear Gd_2O_2 units. Figure 6 schematically describes the dinuclear block of compound **1**, A, together with two other bridging motifs, B and C, corresponding to compounds for which magnetic and structural data are available,[28,30,31] (Table 4). The ferromagnetic compounds **a**−**d**, with bridging motifs of type A, have J_o values between 0.024 and 0.060 cm^{-1} and Gd−O−Gd angle values between 114° and 119°. Centrosymmetric compounds **e**−**h** show a bridging motif B involving two symmetry-related O bridges of type A, plus two syn−syn bidentate carboxylate bridges. In these compounds, the Gd−O−Gd angles in the Gd_2O_2 cores are smaller than 106°, and the interactions are reported to be antiferromagnetic.

The magnitude of the exchange interaction is the result of ferromagnetic and antiferromagnetic contributions. The latter strongly depends on the overlap integral of the chemical path connecting the unpaired spins.[37] Since the ferromagnetic contribution dominates in the compounds with dinuclear units of type A, the overlap integral along the Gd−O−Gd bond should be small. The incorporation of two additional syn−syn bidentate carboxylates in compounds of type B decreases the angles and distances in the tridentate carboxylate oxygen bridge increasing the overlap integral and thus the antiferromagnetic contribution to the exchange coupling, which produces the change of sign of J_o. Compound **i** has a bridge of type C with two tridentate carboxylate oxygens, as in A, but only one syn−syn bidentate carboxylate bridge. In this case, the value of the Gd−O−Gd angle and the distance between the Gd(III) ions falls between those for types A and B, and the ferromagnetic coupling still prevails. The number of case studies available is rather scarce so it is not possible yet to make a quantitative correlation between the

magnitude of the exchange interactions and the geometrical parameters of the bridges. The uncertainties in the values of the coupling constant, J_o, calculated under different approximations is another limitation. However, the trend observed supports the interpretation given above.

In summary, we have characterized two new isostructural lanthanide citrates $[Ln(Hcit)(H_2O)_2 \cdot H_2O]_n$ (Ln = Gd (**1**) and Nd (**2**)) showing Ln_2O_2 blocks as steps in a ladderlike architectural motif. The relatively large difference between the first and second Ln···Ln neighbor distances permits modeling the magnetic data of compound **1** with a dinuclear Hamiltonian, fitted with $J_o = +0.039(4)$ cm^{-1} and $g = 1.995(5)$. A comparison with corresponding values for related gadolinium systems provides a basis for further study of the structural parameters determining the resulting exchange interactions. The main features of the observed EPR powder spectrum can be well explained only assuming dipolar interactions between Gd ions.

Acknowledgment. Financial support from Région Bretagne (France) for the acquisition of the magnetic equipment is greatly acknowledged. We thank to the Spanish Research Council (CSIC) for providing some of us with free-of-charge licenses to the CSD system.[40] The work at INQUIMAE has been supported by PIP 02568. The work at UNL was supported by grants CAI+D-UNL and ANPCyT PICT 06-13872. M.P. and R.C. are members of CONICET.

Supporting Information Available: Crystallographic information in CIF format. This material is available free of charge via the Internet at http://pubs.acs.org.

IC0510056